HHS Public Access

Author manuscript

Biochemistry. Author manuscript; available in PMC 2016 November 17.

Published in final edited form as:

Biochemistry. 2015 November 17; 54(45): 6842–6851. doi:10.1021/acs.biochem.5b01008.

Crystal Structure of the Zorbamycin-Binding Protein ZbmA, the Primary Self-Resistance Element in *Streptomyces flavoviridis* ATCC21892

Jeffrey D. Rudolf[1], **Lance Bigelow**[2], **Changsoo Chang**[2], **Marianne E. Cuff**[2], **Jeremy R. Lohman**[1], **Chin-Yuan Chang**[1], **Ming Ma**[1], **Dong Yang**[1], **Shonda Clancy**[2], **Gyorgy Babnigg**[2], **Andrzej Joachimiak**[2], **George N. Phillips Jr.**[3], and **Ben Shen**[1,4,5,*]

[1]Department of Chemistry, The Scripps Research Institute, Jupiter, FL 33458, USA

[2]Midwest Center for Structural Genomics and Structural Biology Center, Biosciences Division, Argonne National Laboratory, Argonne, IL 60439

[3]BioSciences at Rice and Department of Chemistry, Rice University, Houston, TX 77251

[4]Department of Molecular Therapeutics, The Scripps Research Institute, Jupiter, FL 33458, USA

[5]Natural Products Library Initiative, The Scripps Research Institute, Jupiter, FL 33458, USA

Abstract

The bleomycins (BLMs), tallysomycins (TLMs), phleomycin, and zorbamycin (ZBM) are members of the BLM family of glycopeptide-derived antitumor antibiotics. The BLM-producing *Streptomyces verticillus* ATCC15003 and the TLM-producing *Streptoalloteichus hindustanus* E465-94 ATCC31158 both possess at least two self-resistance elements, an *N*-acetyltransferase and a binding protein. The *N*-acetyltransferase provides resistance by disrupting the metal-binding domain of the antibiotic that is required for activity while the binding protein confers resistance by sequestering the metal-bound antibiotic and preventing drug activation via molecular oxygen. We recently established that the ZBM producer, *Streptomyces flavoviridis* ATCC21892, lacks the *N*-acetyltransferase resistance gene and that the ZBM-binding protein, ZbmA, is sufficient to confer resistance in the producing strain. To investigate the resistance mechanism attributed to ZbmA, we determined the crystal structures of apo and Cu(II)-ZBM-bound ZbmA at the high resolutions of 1.90 Å and 1.65 Å, respectively. Comparison and contrast with other structurally characterized members of the BLM-binding protein family revealed key differences in the protein-ligand binding environment that fine-tunes the ability of ZbmA to sequester metal-bound ZBM and supports drug sequestration as the primary resistance mechanism in the producing organisms of the BLM-family of antitumor antibiotics.

The bleomycin (BLM) family of glycopeptide-derived antibiotics are natural products used in clinical chemotherapy treatments against lymphomas, testicular cancer, and squamous cell carcinomas.[1–4] BLMs cause sequence-specific, metal-dependent oxidative cleavage of

*Corresponding author shenb@scripps.edu. Telephone: (561) 228-2456. Fax: (561) 228-2472.

Notes

The authors declare no competing financial interests.

double-stranded DNA[5, 6] and certain tertiary structures of RNA.[7] BLMs consist of four structural domains: (i) the metal-binding domain containing pyrimidoblamic acid and β-hydroxyhistidine, (ii) the DNA-binding domain comprised of the bithiazole moiety and C-terminal amine, in cooperation with the aminopyrimidine ring, (iii) a linker domain joining the DNA- and metal-binding domains, and (iv) a disaccharide moiety responsible for cell selectivity and impacting DNA cleavage activity.[3, 8–12] Five nitrogen atoms within the metal-binding domain, with the primary amine of the β-aminoalanine moiety as the axial ligand, coordinate iron and oxygen in the active form of the antibiotic (Fig. 1).[13]

The BLMs, tallysomycins (TLMs), phleomycins (PLMs), and zorbamycin (ZBM) are structurally- and functionally-related glycopeptides (Fig. 1).[14–17] The metal-binding domain, including the five metal-binding nitrogens, is strictly conserved in all family members. The three major structural differences within the BLM family of antibiotics are: (i) bithiazole moieties in the BLMs and TLMs versus thiazolinyl-thiazole moieties in the PLMs and ZBM, (ii) a unique terminal amine of ZBM in comparison to the other family members that share many of the same C-terminal amines, and (iii) the same disaccharide moiety consisting of L-gulose-3-*O*-carbamoyl-D -mannose in BLMs, TLMs, and PLMs in contrast to the unique 6-deoxy- L-gulose-containing disaccharide in ZBM; an additional sugar, 4-amino-4,6-dideoxy- L-talose, is also present in the linker domain of TLM.

Antibiotic producers contain intrinsic elements within their genomes that provide self-resistance to the lethal compounds they produce. In addition to the four major mechanisms of resistance to antibiotics – antibiotic modification or destruction, target modification, antibiotic efflux, and metabolic pathway circumvention[18] – antibiotic sequestration is another possible mechanism.[19–21] The bleomycin producer, *Streptomyces verticillus* ATCC15003, contains at least two of these mechanisms.[22, 23] In a unified model for self-resistance to the BLM family of antibiotics, BlmA and BlmB provide the primary and secondary mechanisms of resistance, respectively.[24] BlmA noncovalently binds metal-bound BLMs and sequesters them, preventing the antibiotics from binding to O_2, becoming active, and cleaving DNA.[6, 13, 19] BlmB acetylates the primary amine of the β-aminoalanine moiety of metal-free BLMs preventing the formation of activated BLMs by inhibiting the metal-chelated complex from coordinating to and/or reducing molecular oxygen.[24–28] The biosynthetic gene cluster of TLM from *Streptoalloteichus hindustanus* E465-94 ATCC31158[29] mirrors that of BLM, encoding homologues of both resistance proteins (TlmA and TlmB, respectively). The ZBM producer *Streptomyces flavoviridis* ATCC21892, however, lacks a BlmB homologue in its genome,[24, 30] yet ZbmA is sufficient to provide resistance to ZBM in the producing strain.[24]

After the structure of Shble (i.e., TlmA) from the TLM-producing *S. hindustanus* was reported in 1994 (PDB 1BYL),[31] BLM-binding proteins have been extensively studied resulting in numerous high resolution crystal and NMR solution structures. Apo, BLM-bound, and Cu(II)-BLM-bound structures of BlmA from *S. verticillus* (PDB 1QTO, 1JIE, and 1JIF, respectively)[13, 32] and BlmT from the Tn5 transposon from *Klebsiella pneumoniae* (PDB 1ECS, 1EWJ)[33] revealed that (i) the BLM-binding proteins form two cooperative BLM-binding pockets by dimer formation,[13, 31] (ii) the axial ligand of the metal ion is the primary amine of the β-aminoalanine moiety,[13] (iii) the preferred conformation of the

bithiazole moiety is trans, although both isomers are possible,[13, 33] and (iv) and BLM's bithiazole moiety, long C-terminal amine, and propionamide moiety of pyrimidoblamic acid are important for binding.[13] No structures are reported, however, of the ZBM-binding protein, ZbmA, nor a BLM- or TLM-binding protein complexed with a member of the BLM family possessing a thiazolinyl-thiazole moiety, namely the PLMs or ZBM.

Here, we report the crystal structure of ZbmA, the ZBM-binding protein and primary self-resistance element in *S. flavoviridis* ATCC21892, in both its apo and Cu(II)-ZBM bound forms at 1.90 Å and 1.65 Å, respectively. Our findings unveiled that (i) the overall structure of ZbmA is highly homologous to other BLM-binding proteins, (ii) ZbmA undergoes minor conformational changes upon binding ZBM, and (iii) the binding sites of ZbmA have been fine-tuned to accept the structurally unique ZBM.

MATERIALS AND METHODS

Gene cloning and expression and protein overproduction and purification

Sesame was used as the laboratory information system for project information and reporting to the PSI Target Track Database.[34] The full length *zbmA* gene from *S. flavoviridis* ATCC21892 (NCBI accession, gi: 195970725; locus version: ACG60763) was amplified by PCR from genomic DNA with KOD Hot Start DNA polymerase, amplification buffer supplemented with betaine to a final concentration of 2.5 M, and the following forward and reverse primers, 5′-TACTTCCAATCCAATGCCATGGCCGTATTGCTCTCGGGG-3′ and 5′-TTATCCACTTCCAATGTTAACGAACCGTCCGGGTCGTTTC-3′, respectively. The PCR product was purified, treated with T4 polymerase,[35] cloned into pMCSG57 according to ligation-independent procedures,[36, 37] and transformed into *E. coli* BL21(DE3)-Gold (Stratagene). Protein production, purification, and His_6-tag cleavage were carried out as described previously[38] and resulted in protein with a Ser-Asn-Ala peptide preceding the N-terminal Met. During the first batch of protein production, used for the crystallization of apo ZbmA, methionine biosynthetic inhibitory amino acids (25 mg L^{-1} each of L-valine, L-isoleucine, L-leucine, L-lysine, L-threonine, L-phenylalanine) and L-selenomethionine (SeMet, Medicillin) were added before isopropyl β-D-1-thiogalactopyranoside (IPTG) induction. A second batch of protein was purified for optimization with reductive alkylation and partial proteolysis.[39] For cocrystallization of ZbmA with Cu(II)-ZBM, the inhibitory amino acids and SeMet were not added during protein production. Protein concentrations were determined from the absorbance at 280 nm using a calculated molar absorptivity constant (ε_{280} = 23,490 M^{-1} cm^{-1}).[40] The concentration of pure protein samples used for crystallization was 58.5 mg mL^{-1} for unmodified ZbmA, 49.6 mg mL^{-1} for reductively methylated, 51.0 mg mL^{-1} for reductively ethylated, 46.6 mg mL^{-1} for reductively isopropylated, 51.4 mg mL^{-1} for partial proteolysis (with chymotrypsin, trypsin, or thermolysin), and 41.0 mg mL^{-1} for unmodified ZbmA cocrystallization with Cu(II)-ZBM. Individual aliquots of purified protein were stored at −80 °C until use.

Protein crystallization

ZbmA was screened against several commercially available crystallization conditions including MCSG-1–3 (Microlytic) at 24 °C and 4 °C for the unmodified protein, MCSG-1–4

at 16 °C for the reductively alkylated proteins and protein-ligand complex, and PEG/Ion HT (Hampton Research Corp.) at 16 °C for the partially proteolyzed proteins. The protein-ligand complex was prepared by mixing ZbmA with 10 mM Cu(II)-ZBM at 4 °C for several hours before crystallization. Cu(II)-ZBM was isolated from *S. flavoviridis* SB9001 as previously reported.[17] Vapor-diffusion sitting drops containing 0.4 μ;L of protein and 0.4 μ;L of screening solution were set up in 96-well CrystalQuick plates (Greiner Bio-one) over wells containing 140 μ;L of screening solution using a Mosquito liquid dispenser (TTP Labtech). While crystals were obtained under several conditions, the best apo ZbmA crystal was obtained from the reductively isopropylated ZbmA at 16 °C with a reservoir solution containing 0.8 M ammonium sulfate and 0.1 M sodium citrate, pH 4.0. The best Cu(II)-ZBM-bound ZbmA crystal was obtained at 16 °C with a reservoir solution containing 0.1 M phosphate-citrate, pH 4.2, 40% (v/v) glycerol, and 5% (w/v) polyethylene glycol 1000. The crystals grew within one month and were cryoprotected and flash frozen in liquid nitrogen.

Data collection, structure determination, and refinement

Diffraction data were collected on the 19-BM and 19-ID beamlines of the Structural Biology Center at the Advanced Photon Source.[41] Data were collected to 1.90 Å and 1.65 Å at the peak wavelengths (0.97929 and 0.97918 Å) for the single best apo ZbmA and Cu(II)-ZBM-bound ZbmA crystals, respectively. Data were processed using the HLK-3000 program.[42] For SeMet-labeled apo ZbmA, single-wavelength anomalous diffraction (SAD) was used for phasing and an initial model was built using the program suite HKL-3000. The model was completed manually with Coot.[43] For native Cu(II)-ZBM-bound ZbmA, the structures were determined by molecular replacement using apo ZbmA as the starting model. All final models were refined with Refmac5[44] from the CCP4 suite[45] or PHENIX.[46] The models were analyzed and validated using MolProbity[47] and Coot validation tools.[43] The final atomic coordinates and amplitudes were deposited in the Brookhaven Protein Data Bank, entry codes 4IAG and 5CJ3 for the apo and Cu(II)-ZBM-bound forms of ZbmA, respectively. Figures were prepared using PYMOL (Schrödinger, LLC) and structures were visually examined using a collaborative stereographic system.[48]

RESULTS AND DISCUSSION

Bioinformatics analysis of ZbmA revealing key differences in ligand binding site

An amino acid sequence alignment containing members of the BLM-binding protein family (Fig. 2) showed ZbmA shares high sequence homology with both BlmA (50% identity and 74% similarity) and TlmA (Shble, 56% identity and 74% similarity), yet low homology with the transposon Tn5 homologue BlmT (21% identity and 50% similarity). Given the structural nature of the BLM family of natural products, including the strictly conserved metal-binding domain, many of the residues in ZbmA proposed to bind ZBM are also conserved throughout the BLM-binding family. However, differences in the linker and DNA-binding domains of ZBM likely brought about evolutionary changes to its corresponding resistance protein resulting in a binding protein optimized for ZBM sequestration. Three key residues in ZbmA represent this likely evolutionary optimization: Thr35, Glu47, and Arg98. Sequence alignments and structures of BlmA, TlmA, and BlmT suggest that both Thr35 and Glu47 are in close proximity to the DNA-binding domain of

ZBM, a region with two major differences (i.e., its thiazolinyl-thiazole moiety and unique terminal amine) between ZBM and the other members of the BLM family. The Arg98 counterpart in BlmT, Glu95 (Gly98 in BlmA and TlmA), helps form an outside wall near the linker domain of BLM, foreshadowing a potential interaction of Arg98 in ZbmA with the linker domain of ZBM. Another conspicuous active site residue difference in ZbmA is Gln63 (Ser or Leu in other members). In an attempt to construct a selectable marker for hyperthermophiles, the Shble resistance protein was randomly mutated.[49] Interestingly, the Leu63Gln mutation had a central role in thermostability as it was found in three of the five thermostable mutants. Structural analysis showed that $Gln63_{Shble}$ was involved in an extensive H-bond network. While BlmA and BlmT possess Ser63, which may contribute to a similar H-bond network, ZbmA appears to already have the preferred Gln63.

Crystallization, data collection, and structural refinement

Apo ZbmA crystallized in many conditions; however, the best crystals were obtained from reductively isopropylated ZbmA. It is not clear from the structure why reductive isopropylation lead to the best crystals. However, the single lysine residue is accessible on the surface of the protein and is in close proximity to another isopropyl lysine of a symmetry mate, resulting in crystal contacts. Apo ZbmA crystallized in the space group $P6_522$ with cell dimensions of $a = b = 38.79$ Å × $c = 268.52$ Å and one molecule per asymmetric unit. The structure was solved by Se-SAD with phasing from a single selenomethionine. Data collection and refinement statistics can be found in Table 1. The final refinement statistics are reasonable with an R_{work} of 0.183, R_{free} of 0.231, and resolution of 1.90 Å. Electron density revealed the presence of residues Ala2–Ser122 with residues Ser-2–Met1 and Glu123–Arg132 missing. One molecule of glycerol, eight molecules of 1,2-ethanediol, and 55 water molecules were also visible in the electron density.

The best crystals of Cu(II)-ZBM-bound ZbmA were obtained by using the unmodified ZbmA. Complexed ZbmA crystallized in the space group $P2_12_12_1$ with cell dimensions of $a = 40.74$ Å × $b = 78.99$ Å × $c = 79.54$ Å and two molecules per asymmetric unit. The structure was solved by molecular replacement using apo ZbmA as the starting model. Data collection and refinement statistics can be found in Table 1. The final refinement statistics are reasonable with an R_{work} of 0.176, R_{free} of 0.231, and resolution of 1.65 Å. Electron density revealed the presence of residues $Ser\text{-}2^A$–$Glu123^A$ and $Met1^B$–$Glu126^B$ with residues $Ala124^A$–$Arg132^A$, $Ser\text{-}2^B$–$Ala0^B$, and $Thr126^B$–$Arg132^B$ missing. Two molecules of Cu(II)-ZBM and 165 water molecules were also visible in the electron density. As previously described for Cu(II)-BLM,[13] the Cu(II) ion is chelated by the five metal-binding nitrogens of ZBM and a chloride ion forming a tetragonal bipyramidal coordination complex (Figs. 1 and 3). The electron density for part of the linker domain and thiazolinyl moiety of ZBM shows some discontinuity, whereas the density for the metal-binding domain, disaccharide moiety, 3-aminopropionamidine C-terminal amine, and the thiazole moiety are apparent and clear (Fig. 3). The presence of additional electron density near the terminal amine suggested a secondary conformation for the thiazolinyl-thiazole and 3-aminopropionamidine moieties, modeled in an occupancy of 45%.

The overall structure of ZbmA revealing structural similarity to known BLM-binding proteins

As expected given the conserved nature of the family of BLM-binding proteins, the overall secondary (Fig. 2) and tertiary structure (Fig. 4A) of ZbmA showed high similarity to that of the structurally characterized homologues.[31–33] Superposition of the backbone atoms of Cu(II)-ZBM-bound ZbmA on those of BlmA (PDB 1JIF), TlmA (Shble, PDB 1BYL; thermostable mutant, PDB 1XRK), and BlmT (PDB 1EWJ) gave root-mean-square deviations (RMSD) of 0.523 Å, 0.333 Å, 0.359 Å, and 2.096 Å, respectively, supporting the structural conservation found among all members of the BLM-binding protein family. The topologies of both the monomeric apo ZbmA and the dimeric Cu(II)-ZBM-bound ZbmA are identical with each monomer containing N- and C-terminal domains with β-α-β-β-β topologies. The N-terminal domain, comprised of the α1-helix and a four stranded β-sheet (β1–β4), and the C-terminal domain, comprised of the α2-helix and a five-stranded β-sheet (β5–β9), are joined by a short 3_{10}-helix (η1). The N-terminal β1-strand contributes to dimer formation and stabilization by alternate arm exchange between two ZbmA monomers, as previously described for other BLM- and TLM-binding proteins.[31–33]

ZbmA undergoes minor conformational changes when binding Cu(II)-ZBM

Cu(II)-ZBM-ZbmA forms a dimer with two binding pockets, each consisting of a large concavity and an interfacial groove housing one Cu(II)-ZBM molecule. With the exception of a noncrystallographic 2-fold axis displaying a dimer containing the aforementioned β1-strand alternate arm exchange, the overall structure of ZbmA complexed with Cu(II)-ZBM is nearly identical to apo ZbmA (Fig. 4B). Superposition of the backbone atoms of apo ZbmA with both chains of complexed ZbmA revealed no major conformational changes upon Cu(II)-ZBM binding (RMSDs of chain A and B were 0.147 Å and 0.226 Å, respectively). A major conformational change was seen in BlmA after binding to BLM A2.[13] The β-turn from Ser100 to Gly103 underwent a dramatic loop shift of 5.4 Å and 3.6 Å for the Pro101 in chain A and B, respectively, upon BLM A2 binding. This shift was attributed to Pro101 forming a hydrophobic interaction with the bithiazole moiety in BLM A2 and brought about increased structural rigidity in the β-turn. Upon ZBM binding to ZbmA, the analogous β-turn from Val100 to Gly103 in ZbmA only shifted Pro101 by 0.9 Å. The presence of Trp102 in ZbmA (Ala102 in BlmA) may explain this delicate loop shift. Trp102, in both the apo and complexed forms, lies directly across from Phe38 of the other chain and forms one side of the interfacial groove that binds the thiazolinyl-thiazole moiety (Fig. 4C). The inherent presence of this hydrophobic residue minimizes the need for ZbmA to alter its conformation as Trp102 is already in prime position to interact with the antibiotic. Interestingly, TlmA and BlmT also possess a Trp residue in that position and exhibit similar, relatively minor conformational changes of 2.6 Å and 1.9 Å, respectively.

Inspection of the side chains of ZbmA in the apo and Cu(II)-ZBM bound forms revealed two residues that undergo noteworthy changes upon antibiotic sequestration. The phenyl ring of Phe38, one of the residues forming the thiazolinyl-thiazole-binding groove, rotates ~80° upon binding ZBM (Fig. 4C). This rotation not only widens the groove but sets up sandwich π-stacking interactions with the thiazole moiety of ZBM. In the concavity pocket of the ligand binding site, the long flexible side chain of Arg98 adopts a different rotamer upon

binding to ZBM (Fig. 4C), positioning the guanidinium group near three separate oxygens in the linker domain (see below for detailed description). As none of the other BLM-binding proteins possess an Arg at this position (Gly or Glu), yet each antibiotic has the same three oxygens in the linker domain, Arg98 in ZbmA affords three additional hydrogen bonds, hence additional sites for interacting with the ZBM antibiotic.

Cu(II)-ZBM-ZbmA structure revealing key binding interactions

As seen in previous BLM-binding proteins, the dimer interface of ZbmA, burying almost 4000 $Å^2$ of solvent accessible surface area, creates two antibiotic-binding pockets each consisting of a concavity and an aromatic groove (Fig. 5A).[31–33] The metal-binding domain and disaccharide moiety reside in the concavity. The linker domain, also in the concavity, loses reliable electron density towards the thiazolinyl moiety supporting the flexible and disordered nature of this region (Fig. 3). The C-terminal 3-aminopropionamidine and thiazole moiety showed excellent electron density and was modeled accordingly (mode 1). It was clear, however, from additional unmodeled density that a second conformation was also possible (mode 2). Therefore, both conformations were modeled into each binding site (Fig. 3). While these moieites lie in the aromatic groove in both modes, mode 1 sits deeper in the groove making a number of stabilizing interactions with ZbmA and is likely the preferred binding mode. Over half (~780 $Å^2$) of the total surface area of ZBM (~1530 $Å^2$) is buried through interactions with ZbmA.

As both monomers of ZbmA and both bound molecules of Cu(II)-ZBM show minimal differences, the following descriptions are based on the Cu(II)-ZBM molecule in chain A. The metal-binding domain and sugars of ZBM form an extensive hydrogen bonding network with residues lining the binding pocket and coordinated water molecules (Fig. 5B). These interactions make up the majority of the interactions necessary for ZbmA to sequester the antibiotic. The phenolic oxygen of $Tyr86^A$ and the side chain of $Arg109^A$ interacts with the 4′-hydroxyl of mannose. The side chain of $Tyr86^A$ also hydrogen bonds with the carboxamide oxygen of the pyrimidine ring. The 6′-hydroxyl of mannose coordinates with the carbonyl oxygen of β-hydroxyhistidine through a single hydrogen bonded water molecule. The 3′-*O*-carbamoylmannose moiety appears to be a key proponent in the hydrogen bonding network. Although it is involved in a complicated hydrogen bonding network, $Asp60^A$ is the only residue that directly interacts with it; one of the side chain oxygens of $Asp60^A$ hydrogen bonds with the nitrogen of the carbamoyl group. The other side chain oxygen of $Asp60^A$, the backbone carbonyl oxygen of $Ala89^A$, and the side chain nitrogen of $Gln56^A$, all coordinate waters in the hydrogen bonding network. The carbonyl oxygen of the carbamoyl moiety also appears to form a key hydrogen bonding network with the backbone oxygen of $Asp60^A$, the 3′-hydroxyl of 6-deoxy- L-gulose, and the primary amine of β-aminoalanine. The three backbone carbonyl oxygens of $Pro59^A$, $Thr62^A$, and $Gly113^A$ form hydrogen bonds with the amino group of the pyrimidine ring and both the side chain hydroxyl and backbone oxygen of $Ser52^B$ coordinate a water molecule that hydrogen bonds with the nitrogen of the propionamide moiety. The side chain of $Gln63^A$, the key residue in the thermostable Shble mutant, is in close proximity to the propionamide amide nitrogen, but instead, along with the backbone oxygen of $Asn61^A$, forms a hydrogen bond to a water molecule.

The linker domain shows a limited number of stabilizing interactions, reflecting its disordered nature (Fig. 5C). Arg98^{A}, the residue that rotates upon binding to Cu(II)-ZBM, is the only direct protein-ligand interaction with the linker domain and forms three hydrogen bonds with the 3′-hydroxyl of methylcaproate, and the side chain and backbone carbonyl oxygens of hydroxyvaline. Gln63^{A}, Thr95^{A}, Glu105^{A}, and His117^{A} all line the cavity near the linker domain, but do not appear to make any direct interactions. The 6′-hydroxyl of methylcaproate twists towards the carbonyl oxygen of β-hydroxyhistidine forming an intramolecular hydrogen bond.

The C-terminal thiazolinyl-thiazole and 3-aminopropionamidine moieties reside in a groove created by the dimer interface (Fig. 5C). Trp65^{A}, Trp102^{A}, Phe33^{B}, Phe38^{B}, and Phe49^{B} form the hydrophobic faces of the groove that holds the thiazolinyl-thiazole moiety. The side chain nitrogens of Arg67^{A} hydrogen bond with the carbonyl oxygen of the thiazole ring. Glu32^{B} and Leu121^{A} help form a pocket where the C-terminal amine lies, but the side chain of Glu47^{B} makes the vital interaction with a nitrogen on the amidine functional group.

Comparisons between the ZBM-, TLM-, and BLM-binding proteins revealing ZbmA is fine-tuned to sequester ZBM

An overlay of ZBM (from 5CJ3) and BLM A2 (from 1JIF)[13] reveals little variation between their metal-binding domains and sugar moieties with the main difference a minor displacement of the β-hydroxyhistidine and disaccharide moieties. This results in the carbamoyl moiety of the mannose in ZBM forming a hydrogen bond network to bind with the primary amine of β-aminoalanine instead of an intramolecular hydrogen bond as seen in BlmA (Fig. 5B). The linker domain of BLM mainly interacts with BlmA through water molecules; also a plausible scenario in ZbmA. However, one significant difference is that the flexible Arg98^{A} in ZbmA extends out from the cavity wall to interact with three separate oxygens. Having no side chain, Gly98 in BlmA and TlmA is unable to make these contacts (Fig. 4C). Given the flexibility of the linker domains and C-terminal amines of ZBM and BLM, and consequently incomplete electron densities, it is understandable the biggest variation is in those regions. The one constant feature is that the thiazole in ZBM is positioned in an identical location as the C-terminal thiazole in BLM (Fig. 5D). The nonaromatic thiazolinyl moiety of ZBM sits on the edge of the highly hydrophobic groove, placing the aromatic thiazole between the five aromatic residues, including Trp102^{A}, that form the hydrophobic groove. The excellent electron density of the preferred binding mode for the C-terminal amine of ZBM (Fig. 3E) provides an opportunity to reassess the modeled γ-aminopropyldimethylsulfonium moiety of BLM A2.[13] The crystal structures of BlmA and the thermostable Shble mutant with BLM A2 both lacked electron density for the C-terminal amines.[13, 49] Similarly to ZBM, the C-terminal amine of BLM A2 was modeled into two modes based on the electron density of the bithiazole moiety (Fig. 5D). The tail of one of the conformations was proposed to wrap around placing the sulfonium moiety near the 3-aminopropionamidine of ZBM. In BlmA, electrostatic repulsion shifts the positively charged side chain of Arg47^{B} away from the sulfonium moiety upon BLM A2 binding.[13] In ZbmA, the negatively charged Glu47^{B} requires no conformational shift upon ZBM binding.

CONCLUSION

The BLM family of natural products are structurally complex. One member of this family, ZBM, differs structurally from other members in its disaccharide moiety and linker and DNA-binding domains. Although it is unclear which member of the BLM family is ancestral, evolutionary divergence in the biosynthesis and structure of ZBM likely brought about concomitant evolutionary changes to its corresponding resistance mechanisms.[14, 24] These changes resulted in a binding protein optimized for ZBM sequestration. This study describes the high-resolution crystal structure of the ZBM-binding protein ZbmA, both in its apo and Cu(II)-ZBM-bound forms. Comparison and contrast with other structurally characterized members of the BLM-binding protein family revealed key differences in the protein-ligand binding environment that fine-tunes the ability of ZbmA to sequester Cu(II)-ZBM.

Members of the BLM family are activated by binding a metal(II) ion and molecular oxygen (O_2) that undergoes reduction to form a BLM-metal(III)-OOH complex.[3] With two complementary resistance mechanisms, an *N*-acetyltransferase that disrupts the essential metal-binding domain by modifying the metal-free drug and a binding protein that sequesters the metal-bound drug, the BLM and TLM producing strains are extremely well-equipped to prevent activation of their lethal natural products.[24] In an intriguing example of secondary metabolism and self-resistance evolution, the ZBM producer, *S. flavoviridis* ATCC21892, possesses the binding protein but lacks the *N*-acetyltransferase homologue.[24, 30] Therefore, *S. flavoviridis* foregoes a secondary resistance mechanism and solely relies on the ZbmA binding protein for resistance against ZBM. These insights, the crystal structure of ZbmA, and the fact that Cu(II)-ZBM complexes are isolated, support drug sequestration of metal-bound ZBM as the primary resistance mechanism in *S. flavoviridis*, a model that extends to all producing organisms of the BLM-family of antitumor antibiotics.[24]

Acknowledgments

Funding

This work is supported in part by National Institute of General Medical Sciences Protein Structure Initiative grants GM098248 (GNP) and GM094585 (AJ), National Institutes of Health grants CA094426 (BS) and GM109456 (GNP), and the use of Structural Biology Center beamlines at the Advanced Photon Source was supported by U.S. Department of Energy, Office of Biological and Environmental Research grant DE-AC02-06CH11357 (MC and AJ).

References

1. Bayer RA, Gaynor ER, Fisher RI. Bleomycin in non-Hodgkin's lymphoma. Semin Oncol. 1992; 19:46–52. 43. [PubMed: 1384144]
2. Einhorn LH. Curing metastatic testicular cancer. Proc Natl Acad Sci USA. 2002; 99:4592–4595. [PubMed: 11904381]
3. Chen J, Stubbe J. Bleomycins: towards better therapeutics. Nat Rev Cancer. 2005; 5:102–112. [PubMed: 15685195]
4. Galm U, Hager MH, Van Lanen SG, Ju J, Thorson JS, Shen B. Antitumor antibiotics: bleomycin, enediynes, and mitomycin. Chem Rev. 2005; 105:739–758. [PubMed: 15700963]

5. Burger RM, Peisach J, Horwitz SB. Activated bleomycin. A transient complex of drug, iron, and oxygen that degrades DNA. J Biol Chem. 1981; 256:11636–11644. [PubMed: 6170635]
6. Stubbe J, Kozarich JW. Mechanisms of bleomycin-induced DNA degradation. Chem Rev. 1987; 87:1107–1136.
7. Carter BJ, De Vroom E, Long EC, Van der Marel GA, Van Boom JH, Hecht SM. Site-specific cleavage of RNA by iron(II)·bleomycin. Proc Natl Acad Sci USA. 1990; 87:9373–9377. [PubMed: 1701259]
8. Boger DL, Cai H. Review of bleomycin: synthetic and mechanistic studies. Angew Chem, Int Ed. 1999; 38:448–476.
9. Hecht SM. Bleomycin: New perspectives on the mechanism of action. J Nat Prod. 2000; 63:158–168. [PubMed: 10650103]
10. Chapuis JC, Schmaltz RM, Tsosie KS, Belohlavek M, Hecht SM. Carbohydrate dependent targeting of cancer cells by bleomycin-microbubble conjugates. J Am Chem Soc. 2009; 131:2438–2439. [PubMed: 19187019]
11. Yu Z, Schmaltz RM, Bozeman TC, Paul R, Rishel MJ, Tsosie KS, Hecht SM. Selective tumor cell targeting by the disaccharide moiety of bleomycin. J Am Chem Soc. 2013; 135:2883–2886. [PubMed: 23379863]
12. Huang SX, Feng Z, Wang L, Galm U, Wendt-Pienkowski E, Yang D, Tao M, Coughlin JM, Duan Y, Shen B. A designer bleomycin with significantly improved DNA cleavage activity. J Am Chem Soc. 2012; 134:13501–13509. [PubMed: 22831455]
13. Sugiyama M, Kumagai T, Hayashida M, Maruyama M, Matoba Y. The 1.6-Å crystal structure of the copper(II)-bound bleomycin complexed with the bleomycin-binding protein from bleomycin-producing *Streptomyces verticillus*. J Biol Chem. 2002; 277:2311–2320. [PubMed: 11706014]
14. Galm U, Wendt-Pienkowski E, Wang L, Huang SX, Unsin C, Tao M, Coughlin JM, Shen B. Comparative analysis of the biosynthetic gene clusters and pathways for three structurally related antitumor antibiotics: bleomycin, tallysomycin, and zorbamycin. J Nat Prod. 2011; 74:526–536. [PubMed: 21210656]
15. Konishi M, Saito K, Numata K, Tsuno T, Asama K, Tsukiura H, Naito T, Kawaguchi H. Tallysomycin, a new antitumor antibiotic complex related to bleomycin. II. Structure determination of tallysomycins A and B. J Antibiot. 1977; 30:789–805. [PubMed: 591444]
16. Takita T, Muraoka Y, Nakatani T, Fujii A, Umezawa Y, Naganawa H, Umezawa H. Chemistry of bleomycin. XIX. Revised structures of bleomycin and phleomycin. J Antibiot. 1978; 31:801–804. [PubMed: 80403]
17. Wang L, Yun BS, George NP, Wendt-Pienkowski E, Galm U, Oh TJ, Coughlin JM, Zhang G, Tao M, Shen B. Glycopeptide Antitumor Antibiotic Zorbamycin from *Streptomyces flavoviridis* ATCC 21892: Strain Improvement and Structure Elucidation. J Nat Prod. 2007; 70:402–406. [PubMed: 17311457]
18. Wright GD. Molecular mechanisms of antibiotic resistance. Chem Commun. 2011; 47:4055–4061.
19. Gatignol A, Durand H, Tiraby G. Bleomycin resistance conferred by a drug-binding protein. FEBS Lett. 1988; 230:171–175. [PubMed: 2450783]
20. Reynolds PE. Structure, biochemistry, and mechanism of action of glycopeptide antibiotics. Eur J Clin Microbiol Infect Dis. 1989; 8:943–950. [PubMed: 2532132]
21. Hayes JD, Wolf CR. Molecular mechanisms of drug resistance. Biochem J. 1990; 272:281–295. [PubMed: 1980062]
22. Sugiyama M, Thompson CJ, Kumagai T, Suzuki K, Deblaere R, Villarroel R, Davies J. Characterization by molecular cloning of two genes from *Streptomyces verticillus* encoding resistance to bleomycin. Gene. 1994; 151:11–16. [PubMed: 7530224]
23. Du L, Sanchez C, Chen M, Edwards DJ, Shen B. The biosynthetic gene cluster for the antitumor drug bleomycin from *Streptomyces verticillus* ATCC15003 supporting functional interactions between nonribosomal peptide synthetases and a polyketide synthase. Chem Biol. 2000; 7:623–642. [PubMed: 11048953]
24. Coughlin JM, Rudolf JD, Wendt-Pienkowski E, Wang L, Unsin C, Galm U, Yang D, Tao M, Shen B. BlmB and TlmB provide resistance to the bleomycin family of antitumor antibiotics by *N*-

acetylating metal-free bleomycin, tallysomycin, phleomycin, and zorbamycin. Biochemistry. 2014; 53:6901–6909. [PubMed: 25299801]

25. Oppenheimer NJ, Rodriguez LO, Hecht SM. Metal binding to modified bleomycins. Zinc and ferrous complexes with an acetylated bleomycin. Biochemistry. 1980; 19:4096–4103. [PubMed: 6157406]
26. Sugiyama M, Kumagai T, Shionoya M, Kimura E, Davies JE. Inactivation of bleomycin by an *N*-acetyltransferase in the bleomycin-producing strain *Streptomyces verticillus*. FEMS Microbiol Lett. 1994; 121:81–86. [PubMed: 7521855]
27. Matsuo H, Mochizuki H, Davies J, Sugiyama M. Production of bleomycin *N*-acetyltransferase in *Escherichia coli* and *Streptomyces verticillus*. FEMS Microbiol Lett. 1997; 153:83–88. [PubMed: 9252576]
28. Oda K, Matoba Y, Noda M, Kumagai T, Sugiyama M. Catalytic mechanism of bleomycin *N*-acetyltransferase proposed on the basis of its crystal structure. J Biol Chem. 2010; 285:1446–1456. [PubMed: 19889644]
29. Tao M, Wang L, Wendt-Pienkowski E, George NP, Galm U, Zhang G, Coughlin JM, Shen B. The tallysomycin biosynthetic gene cluster from *Streptoalloteichus hindustanus* E465-94 ATCC 31158 unveiling new insights into the biosynthesis of the bleomycin family of antitumor antibiotics. Mol BioSyst. 2007; 3:60–74. [PubMed: 17216057]
30. Galm U, Wendt-Pienkowski E, Wang L, George Nicholas P, Oh T-J, Yi F, Tao M, Coughlin Jane M, Shen B. The biosynthetic gene cluster of zorbamycin, a member of the bleomycin family of antitumor antibiotics, from *Streptomyces flavoviridis* ATCC 21892. Mol Biosyst. 2009; 5:77–90. [PubMed: 19081934]
31. Dumas P, Bergdoll M, Cagnon C, Masson JM. Crystal structure and site-directed mutagenesis of a bleomycin resistance protein and their significance for drug sequestering. Embo J. 1994; 13:2483–2492. [PubMed: 7516875]
32. Kawano Y, Kumagai T, Muta K, Matoba Y, Davies J, Sugiyama M. The 1.5 Å crystal structure of a bleomycin resistance determinant from bleomycin-producing *Streptomyces verticillus*. J Mol Biol. 2000; 295:915–925. [PubMed: 10656800]
33. Maruyama M, Kumagai T, Matoba Y, Hayashida M, Fujii T, Hata Y, Sugiyama M. Crystal structures of the transposon Tn5-carried bleomycin resistance determinant uncomplexed and complexed with bleomycin. J Biol Chem. 2001; 276:9992–9999. [PubMed: 11134052]
34. Zolnai Z, Lee PT, Li J, Chapman MR, Newman CS, Phillips GN Jr, Rayment I, Ulrich EL, Volkman BF, Markley JL. Project management system for structural and functional proteomics: Sesame. J Struct Funct Genomics. 2003; 4:11–23. [PubMed: 12943363]
35. Dieckman L, Gu M, Stols L, Donnelly MI, Collart FR. High throughput methods for gene cloning and expression. Protein Expression Purif. 2002; 25:1–7.
36. Eschenfeldt WH, Stols L, Millard CS, Joachimiak A, Donnelly MI. A family of LIC vectors for high-throughput cloning and purification of proteins. Methods Mol Biol. 2009; 498:105–115. [PubMed: 18988021]
37. Aslanidis C, De Jong PJ. Ligation-independent cloning of PCR products (LIC-PCR). Nucleic Acids Res. 1990; 18:6069–6074. [PubMed: 2235490]
38. Lohman JR, Ma M, Cuff ME, Bigelow L, Bearden J, Babnigg G, Joachimiak A, Phillips GN Jr, Shen B. The crystal structure of BlmI as a model for nonribosomal peptide synthetase peptidyl carrier proteins. Proteins Struct Funct, Bioinf. 2014; 82:1210–1218.
39. Kim Y, Babnigg G, Jedrzejczak R, Eschenfeldt WH, Li H, Maltseva N, Hatzos-Skintges C, Gu M, Makowska-Grzyska M, Wu R, An H, Chhor G, Joachimiak A. High-throughput protein purification and quality assessment for crystallization. Methods. 2011; 55:12–28. [PubMed: 21907284]
40. Gill SC, Von Hippel PH. Calculation of protein extinction coefficients from amino acid sequence data. Anal Biochem. 1989; 182:319–326. [PubMed: 2610349]
41. Rosenbaum G, Alkire RW, Evans G, Rotella FJ, Lazarski K, Zhang RG, Ginell SL, Duke N, Naday I, Lazarz J, Molitsky MJ, Keefe L, Gonczy J, Rock L, Sanishvili R, Walsh MA, Westbrook E, Joachimiak A. The structural biology center 191D undulator beamline: facility specifications and protein crystallographic results. J Synchrotron Radiat. 2006; 13:30–45. [PubMed: 16371706]

42. Minor W, Cymborowski M, Otwinowski Z, Chruszcz M. HKL-3000: the integration of data reduction and structure solution - from diffraction images to an initial model in minutes. Acta Crystallogr, Sect D Biol Crystallogr. 2006; D62:859–866. [PubMed: 16855301]
43. Emsley P, Lohkamp B, Scott WG, Cowtan K. Features and development of Coot. Acta Crystallogr Sect D Biol Crystallogr. 2010; 66:486–501. [PubMed: 20383002]
44. Murshudov GN, Vagin AA, Dodson EJ. Refinement of macromolecular structures by the maximum-likelihood method. Acta Crystallogr, Sect D Biol Crystallogr. 1997; D53:240–255. [PubMed: 15299926]
45. Winn MD, Ballard CC, Cowtan KD, Dodson EJ, Emsley P, Evans PR, Keegan RM, Krissinel EB, Leslie AGW, McCoy A, McNicholas SJ, Murshudov GN, Pannu NS, Potterton EA, Powell HR, Read RJ, Vagin A, Wilson KS. Overview of the CCP4 suite and current developments. Acta Crystallogr Sect D Biol Crystallogr. 2011; 67:235–242. [PubMed: 21460441]
46. Adams PD, Afonine PV, Bunkoczi G, Chen VB, Davis IW, Echols N, Headd JJ, Hung LW, Kapral GJ, Grosse-Kunstleve RW, McCoy AJ, Moriarty NW, Oeffner R, Read RJ, Richardson DC, Richardson JS, Terwilliger TC, Zwart PH. PHENIX: a comprehensive Python-based system for macromolecular structure solution. Acta Crystallogr Sect D Biol Crystallogr. 2010; 66:213–221. [PubMed: 20124702]
47. Chen VB, Arendall WB III, Headd JJ, Keedy DA, Immormino RM, Kapral GJ, Murray LW, Richardson JS, Richardson DC. MolProbity: all-atom structure validation for macromolecular crystallography. Acta Crystallogr Sect D Biol Crystallogr. 2010; 66:12–21. [PubMed: 20057044]
48. Yennamalli R, Arangarasan R, Bryden A, Gleicher M, Phillips GN Jr. Using a commodity high-definition television for collaborative structural biology. J Appl Crystallogr. 2014; 47:1153–1157. [PubMed: 24904249]
49. Brouns SJJ, Wu H, Akerboom J, Turnbull AP, de Vos WM, van der Oost J. Engineering a selectable marker for hyperthermophiles. J Biol Chem. 2005; 280:11422–11431. [PubMed: 15640151]
50. Edgar RC. MUSCLE: multiple sequence alignment with high accuracy and high throughput. Nucleic Acids Res. 2004; 32:1792–1797. [PubMed: 15034147]
51. Gouet P, Courcelle E, Stuart DI, Metoz F. ESPript: analysis of multiple sequence alignments in PostScript. Bioinformatics. 1999; 15:305–308. [PubMed: 10320398]
52. Robert X, Gouet P. Deciphering key features in protein structures with the new ENDscript server. Nucleic Acids Res. 2014; 42:W320–W324. [PubMed: 24753421]

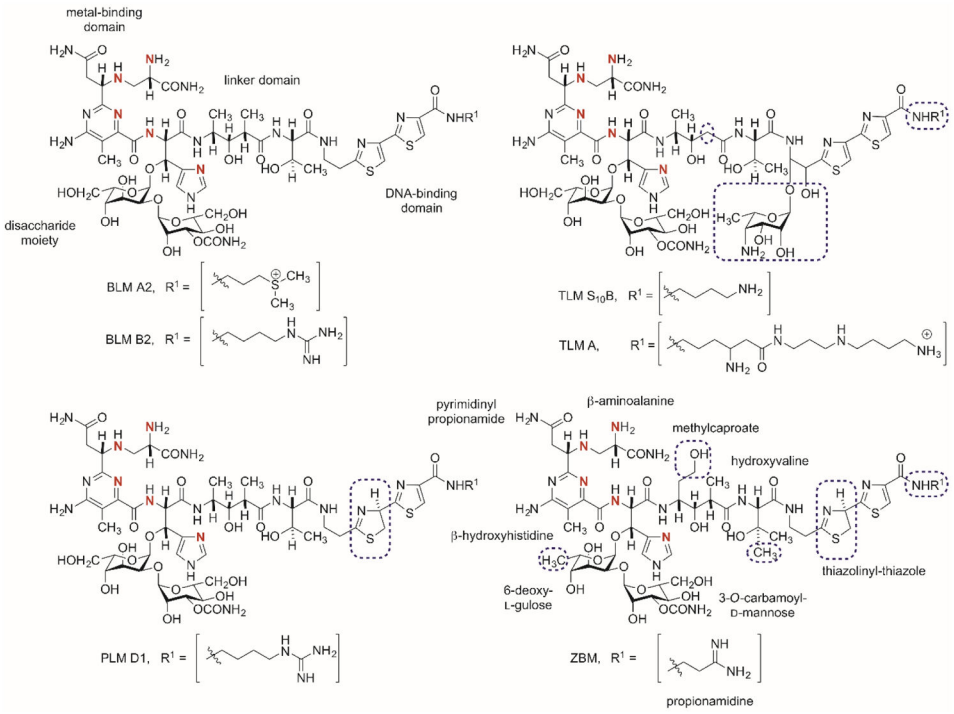

Figure 1.

Structures of selected members of the BLM family of antitumor antibiotics. The five nitrogen atoms that coordinate the metal ion are bolded in red and structural differences between the antibiotics are highlighted with dotted blue boxes. The four structural domains of BLMs and the structural components of ZBM are labeled.

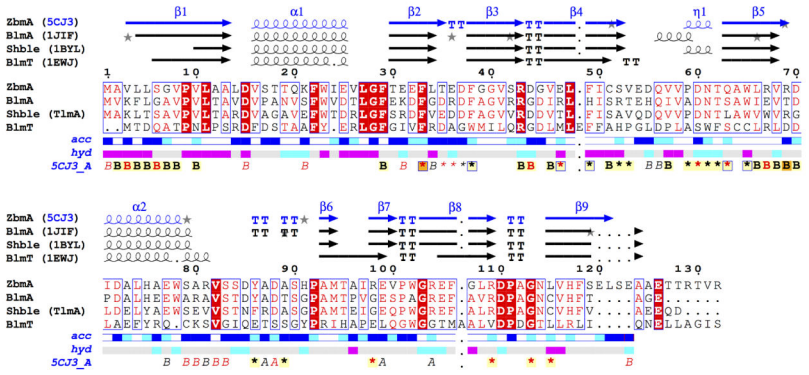

Figure 2.

Sequence alignment of selected BLM-binding proteins that have been structurally characterized. Aligned residues are colored based on level of conservativity (red box with white character is strict identity, red character is similarity, blue frame is similarity across groups). Corresponding secondary structures are depicted above the sequence alignment with gray stars representing residues with multiple conformations. The accessible surface area (*acc*; white are buried residues, cyan are intermediate, blue are accessible), hydropathy (*hyd*; pink are hydrophobic residues, gray are intermediate, cyan are hydrophilic), and protein-ligand contacts of Cu(II)-ZBM-bound ZbmA (A, B, and * with yellow backgrounds are non-crystallographic contacts with chain A, chain B, or ZBM, respectively; *A*, *B*, and * are crystallographic contacts; orange background signifies both non- and crystallographic contacts, red is < 3.2 Å, black is 3.2 – 5.0 Å, blue frame signifies both protein-protein and protein-ligand contacts) from 5CJ3 are depicted below the sequence alignment. The alignment was created with MUSCLE[50] and rendered with ESPript 3.0[51] and ENDscript 2.0.[52]

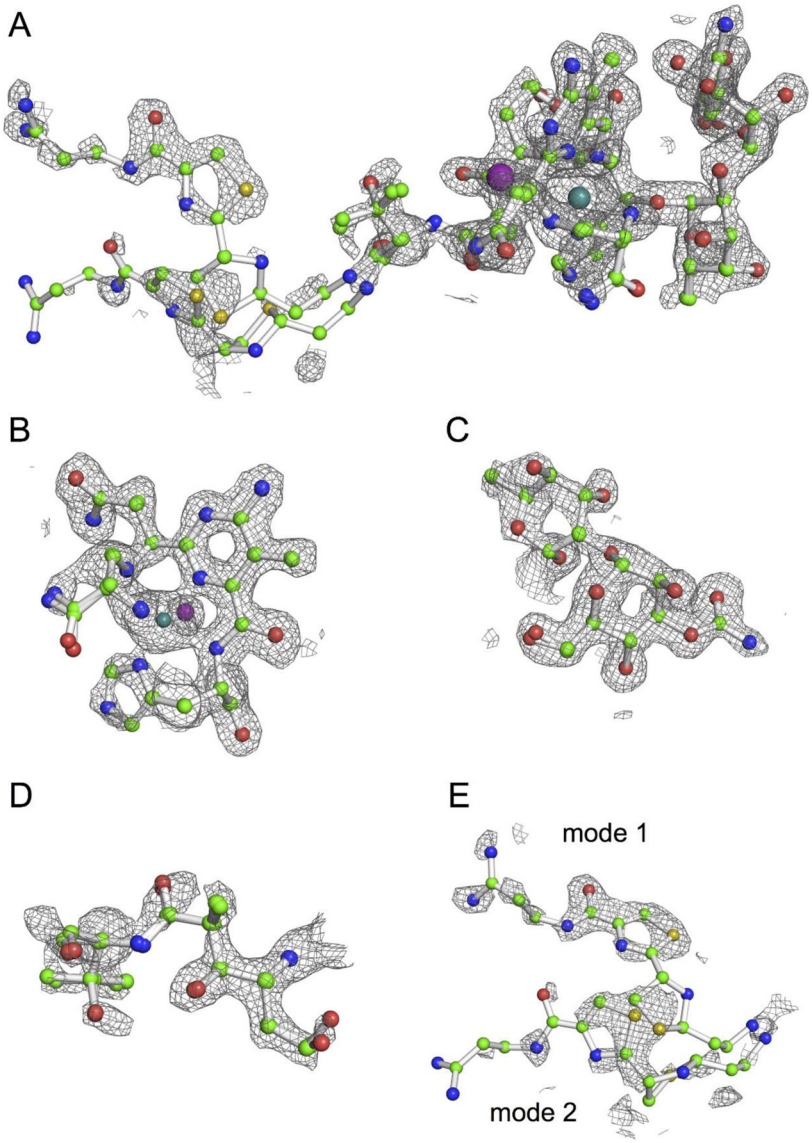

Figure 3.

Electron density map for Cu(II)-BLM. The 2mF_o – DF_c omit map for the ZbmA-Cu(II)-ZBM complex in chain A with a 1.0σ contour (gray). Copper and chloride atoms are shown in teal and purple, respectively. (A) Overall structure of Cu(II)-ZBM. (B) Metal-binding domain comprised of β-aminoalanine, pyrimidylpropionamide, and β-hydroxyhistidine. (C) Unique disaccharide of 6-deoxy- L-gulose-3-*O*-carbamoyl- D-mannose. (D) Linker domain containing methylcaproate and hydroxyvaline. (E) Two binding modes for the DNA-binding domain comprised of the thiazolinyl-thiazole and 3-aminopropionamidine moieties.

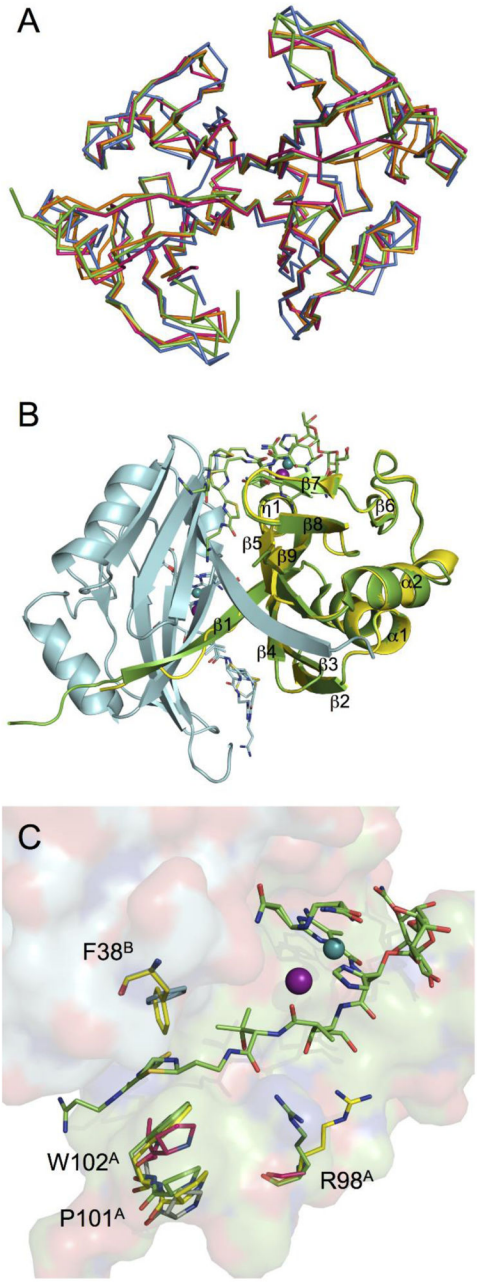

Figure 4.

Overall structure of ZbmA and comparison of the apo and Cu(II)-ZBM-bound structures. (A) Superposition of ZbmA (green, 5CJ3) with BlmA (magenta, 1JIF), TlmA (orange, 1BYL), and BlmT (blue, 1EWJ). (B) Superposition of apo ZbmA monomer (yellow, 4IAG) with the Cu(II)-ZBM-bound ZbmA dimer (chain A green, chain B cyan, 5CJ3). The secondary structure features are labeled as depicted in Fig. 2. The ZBM molecules are shown as sticks with copper and chloride atoms shown as teal and purple spheres, respectively. (C) Differences between the apo and Cu(II)-ZBM-bound ZbmA structures. The coloring scheme is the same as in (B), with the addition of apo BlmA (gray, 1QTO) and

Cu(II)-BLM A2-bound BlmA (magenta, 1JIF) shown for comparison. The side chains of both F38 and R98 rotate upon binding Cu(II)-ZBM to form interactions with the antibiotic. In contrast to BlmA, the loop including P101 and W102 in ZbmA undergoes only a minor shift due to the inherent presence of W102 (A102 in BlmA) along the thiazole-binding groove. The second binding mode of the linker and DNA-binding domains for ZBM was removed for clarity. The surface of the ZbmA dimer is shown in the background.

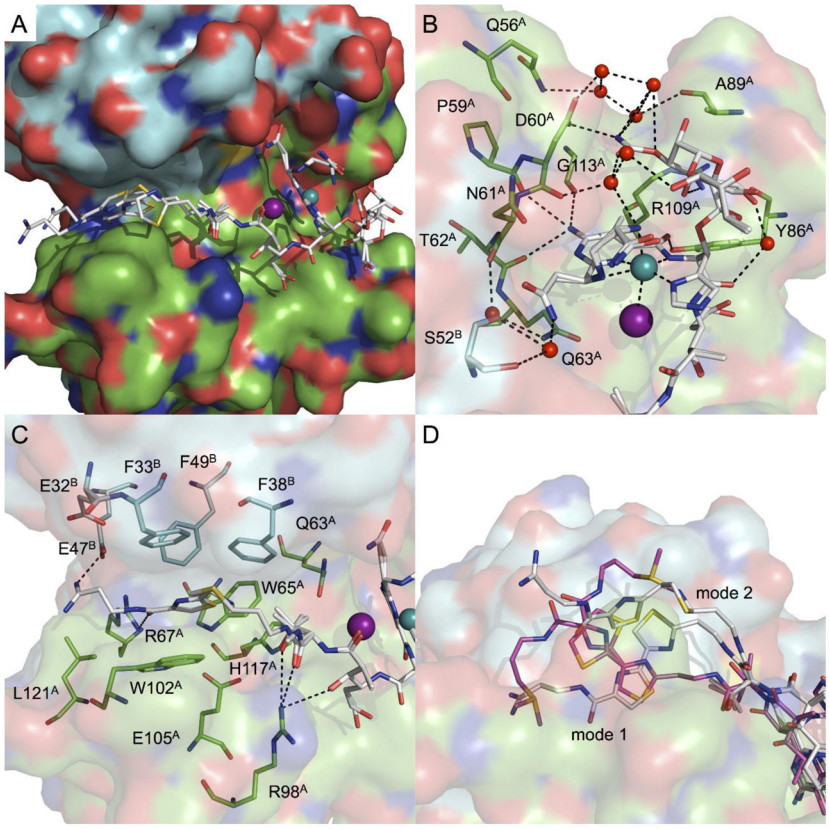

Figure 5.

Binding modes of Cu(II)-ZBM with ZbmA. (A) Overall view of the binding modes of Cu(II)-ZBM in the dimer interface of ZbmA. ZBM (white sticks) with copper and chloride atoms shown as teal and purple spheres, respectively, depicted with the surface of chains A (green) and B (cyan). The metal-binding and linker domains, along with the disaccharide moiety resides in the large concavity. The DNA-binding domain resides in the interfacial groove. (B) Hydrogen-bonding network between ZbmA and the metal-binding domain and disaccharide moiety of Cu(II)-ZBM. Hydrogen bonds are shown as dotted, black lines. (C) Hydrogen-bonding, π-stacking, and hydrophobic interactions between ZbmA and the linker and DNA-binding domains of ZBM. $R98^{A}$ and $E47^{B}$, unique to ZbmA, make key hydrogen bonds with ZBM. $W102^{A}$ is perfectly positioned for sandwich stacking with the thiazole of ZBM. (D) The two binding modes of Cu(II)-ZBM in ZbmA overlayed with the two binding modes of Cu(II)-BLM A2 (1JIF). The thiazole of ZBM (mode 1) and the penultimate thiazole of BLM A2 overlap with each other and reside deep within the aromatic groove. The thiazolinyl-thiazole and 3-aminopropionamidine moieties of ZBM (mode 1) lay completely within the groove; only the thiazole moiety of ZBM (mode 2) resides in the groove.

Table 1

Data Collection and Refinement Statistics

Data set	Apo	WT-Cu(II)-ZBM
Space group	$P6_522$	$P2_12_12_1$
Unit cell	$a = b = 38.79$ Å, $c = 268.52$ Å; α = β = 90°, γ = 120°	$a = 40.74$ Å, $b = 78.99$ Å, $c = 79.54$ Å; α = β = γ = 120°
Wavelength (Å)	0.97929	0.97918
Resolution range (Å)[a]	32.59 – 1.90 (1.93 – 1.90)	35.52 – 1.65 (1.66 – 1.65)
Unique reflections	10484 (460)	29473 (603)
Multiplicity	9.7 (4.0)	7.9 (5.6)
Completeness (%)	98.5 (87.5)	93.0 (79.8)
I/σ_I	33.0 (2.2)	34.7 (5.3)
Wilson B-factor	28.2	12.66
R_{merge} (%)[b]	6.8 (43.4)	5.7 (37.4)
R_{meas} (%)[c]	7.3	6.1
$CC_{1/2}$	0.795	0.931
CC*[d]	0.941	0.982
Phasing and refinement		
Resolution (Å)	32.59 – 1.90 (1.95 – 1.90)	35.52 – 1.65 (1.67 – 1.65)
Number of reflections	10242 (639)	29164 (1989)
R_{work}/R_{free} (%)	18.3/23.1 (28.5/36.8)	17.6/21.3 (19.5/27.1)
Number of atoms	946	2575
Residues		
Macromolecules	121	270
Ligand/ion	9	6
Water	55	165
RMSD bond (Å)	0.016	0.013
RMSD angle (°)	1.836	1.788
Ramachandran plot (%)[e]		
Favored	98.4	98.9
Outliers	0.0	0.0
Clashscore	10.1	2.52
Ligands RSCC[f]	-	0.84
Average B-factor	38.3	17.5
Macromolecules	37.0	16.0
Ligands	49.2	21.7
Water	48.0	26.1
PDB ID	4IAG	5CJ3

[a] Numbers in parentheses are values for the highest-resolution bin

[b] $R_{merge} = \Sigma_{hkl}\Sigma_i|I_i(hkl) - \langle I(hkl)\rangle|/\Sigma_{hkl}\Sigma_i I_i(hkl)$, where $I_i(hkl)$ is the ith observation of reflection hkl, and $\bar{I}(hkl)$ is the weighted average intensity for all observations i of reflection hkl

[c] $R_{meas} = \Sigma_{hkl} (N/(N-1)^{1/2}) \Sigma_i |I_i(hkl) - \bar{I}(hkl)| / \Sigma_{hkl} \Sigma_i I_i(hkl)$

[d] $CC^* = (2CC_{1/2}/(1 + CC_{1/2}))^{1/2}$

[e] As defined by MolProbity

[f] Ligand RSCC: ZBM real-space correlation coefficient